

An interband cascade laser-based in situ absorption sensor for nitric oxide in combustion exhaust gases

O. Diemel¹ · J. Pareja^{2,3} · A. Dreizler^{2,3} · S. Wagner¹ 

Received: 7 February 2017 / Accepted: 2 May 2017 / Published online: 9 May 2017
© Springer-Verlag Berlin Heidelberg 2017

Abstract A direct absorption nitric oxide sensor for combustion exhaust gas measurements, based on an interband cascade laser operating at 5.2 μm , is presented. The sensor was applied to the hot air co-flow of an auto-ignition test rig (800–1300 K), which contains nitric oxide mole fractions of the order of 1 mol%, due to prior microwave plasma heating. The effect of non-uniform temperature along the beam path, on both absorption line strength and gas density, was included in mole fraction measurements at various co-flow temperatures and velocities. At an absorption length of only 82 mm, a noise-limited detection limit of 30 ppm with a 10 ms observation time was achieved at 800 K. The results were compared in detail to previously measured mole fractions, using a sampling gas analyzer.

1 Introduction

Nitric oxide (NO) is one of the major pollutants from the combustion of fossil fuels [1]. It plays an important role in atmospheric physics and contributes to ozone depletion in the stratosphere, formation of ground-level ozone, and acid rain [2]. Furthermore, the presence of NO in exhaled human breath is known to correlate with the inflammatory

status of pulmonary disorders such as asthma [3]. Trace gas detection in related applications is commonly done by diode laser-based absorption spectroscopy, due to its high selectivity and sensitivity [4, 5].

NO absorption sensors and measurements have been widely reported in the literature, probing electronic transitions in the ultraviolet [6], the second and first overtone vibrational bands at 1.8 and 2.65 μm , respectively [7, 8], as well as the fundamental band at 5.3 μm [9]. Even though the line strengths are largest for the electronic transitions, generation of tunable and narrowband UV radiation is fairly complex, and few in situ measurements have been reported [10, 11]. Owing to the availability of thermoelectrically cooled detectors and light sources in the mid-infrared, namely Quantum Cascade Lasers [12], virtually all recently presented NO absorption spectrometers are based on fundamental band transitions [13–30]. Most of these spectrometers are trace gas sensors which are cavity-enhanced [14, 17, 18, 22], use multi-pass cells [13, 19–21, 24], or photoacoustic detection [15, 23, 30] to achieve ppbv and even sub ppbv detection limits in a sampled gas probe at room temperature and/or under reduced pressure, proposing applications in breath analysis and atmospheric sensing.

In situ absorption measurements of NO in combustion environments are scarce in the literature. Weber et al. used a continuous wave (cw) QCL at ~ 100 K operating temperature to measure bag-sampled vehicle exhaust emissions in a 100 m Herriott cell at a pressure of 100 Torr [24]. Jágerská et al. presented time-resolved measurements at an automotive test bench, while the exhaust gas was diluted and sampled in a Herriott cell [13]. They employed a pulsed dual-wavelength QCL at room temperature, for simultaneous NO and NO₂ detection. Wehe et al. measured NO in the exhaust duct of a C₂H₄–air flame at temperatures of ~ 600 K, using a pulsed

✉ S. Wagner
wagner@rsm.tu-darmstadt.de

¹ High Temperature Process Diagnostics Group, Technische Universität Darmstadt, 64289 Darmstadt, Germany

² Reaktive Strömungen und Messtechnik, Technische Universität Darmstadt, 64289 Darmstadt, Germany

³ Darmstadt Graduate School of Excellence Energy Science and Engineering, Technische Universität Darmstadt, Jovanka-Bontschits-Straße 2, 64287 Darmstadt, Germany

QCL near room temperature [27]. Wysocki et al. presented a QCL spectrometer for NO monitoring in industrial exhaust systems, based on an original pulsed detection scheme to achieve fast wavelength tuning [28]. The sensor was validated by means of a laboratory gas cell at atmospheric pressure and temperatures of up to 630 K, but no in situ exhaust application was shown. Chao et al. used a cw external-cavity QCL in direct absorption [25] and WMS [26] operation for real-time in situ NO monitoring in the exhaust of a pulverized-coal-fired power plant.

A viable alternative to QCLs in the wavelength region from about 3–6 μm is Interband Cascade Lasers [31, 32]. Their threshold drive powers are far lower than those of QCLs, making stable operation in harsh environments less intricate. Modern distributed feedback (DFB) ICLs can provide monomode cw emission at room temperature and have been successfully applied in absorption spectroscopy [33–37].

In this paper, we report on the development of a direct absorption NO sensor based on a 5.2 μm DFB ICL [38] for exhaust gas measurements with millisecond time resolution. Particular care was taken in the selection of the absorption feature at 1929 cm^{-1} , to minimize overlapping with transitions of other exhaust gas species. The sensor was used for in situ mole fraction measurements of NO in the plasma-heated air co-flow (800–1300 K) of a laboratory auto-ignition test rig [39]. The test rig targets fundamental research in turbulence–chemistry interactions during auto-ignition processes, relevant for a variety of combustion applications, such as diesel and homogeneous charge compression ignition engines. The measured NO concentrations were corrected for temperature inhomogeneities along the beam path and show good agreement with previously conducted measurements using an extractive gas analyzer [39]. The ICL as well as the infrared detector was operated in close proximity to the test rig (~ 1 m) without noticeable stability problems. Although the measurements in this paper were made during steady-state operation of the test rig without fuel injection, the spectrometer could potentially be applied during auto-ignition operation as well, since it is non-invasive. Furthermore, the detection of concentration transients during ignition becomes feasible with the absorption sensor, in contrast to sampling gas analyzers, which usually have response times of several seconds.

2 Direct TDLAS

2.1 Measurement principle

Direct Absorption (DA) Spectroscopy was applied for the determination of NO mole fractions. The method relies

on measuring the spectral transmission of a monochromatic light source at frequency ν through the probed gas volume. The frequency- and time-dependent extinction at an optical path length of L is described by the Beer–Lambert law, with incident and attenuated intensity I_0 and I , respectively [40]:

$$I(\nu, t) = I_0(\nu, t) \times Tr(t) \times \exp \left[- \sum_j S_j(T) \times \phi_j(\nu - \nu_{0,j}, T, p) \times n \times L \right] + E(t). \quad (1)$$

Broadband attenuation due to, e.g., particles or optical elements is considered by $Tr(t)$, while $E(t)$ accounts for thermal background radiation. The temperature-dependent line strength $S_j(T)$ of molecular transition j , centered at frequency $\nu_{0,j}$, is in this case normalized to the absorber number density n . The normalized line shape function ϕ_j is dependent on temperature T and total gas pressure p due to collisional and Doppler broadening.

By applying a sufficiently broad spectral tuning $\nu(t)$ to the light source, the line shape function can be eliminated from Eq. (1) by integration over time. Using the ideal gas law together with Eq. (1) then yields the absorber mole fraction χ :

$$\chi = - \frac{k_B T}{pL \sum_j S_j(T)} \int \ln \left[\frac{I(\nu, t) - E(t)}{I_0(\nu, t) \times Tr(t)} \right] \frac{\partial \nu}{\partial t} dt. \quad (2)$$

The laser tuning coefficient $\partial \nu / \partial t$ can be obtained prior to the in situ measurements by an interferometric characterization.

Equation (2) presumes a homogeneous temperature of the probed gas. In case of a temperature distribution, the mean temperature along the light path can be employed, if $S_j(T)$ behaves linearly for the given temperature range. As $S_j(T)$ is in general not linear, this is approximation will fail for large temperature differences. In this case, successive execution of the Beer–Lambert law for path sections L_i with local gas temperatures T_i allows for a more accurate formulation of Eq. (2):

$$\chi = - \left[p \sum_i L_i \frac{\sum_j S_j(T_i)}{k_B T_i} \right]^{-1} \int \ln \left[\frac{I(\nu, t) - E(t)}{I_0(\nu, t) \times Tr(t)} \right] \frac{\partial \nu}{\partial t} dt. \quad (3)$$

In this work, Eq. (3) was applied for the mole fraction measurements of NO. Due to the high repetition frequency of the spectral tuning (2 kHz), $E(t)$ was assumed to be constant over the integration time in Eq. (3). The integral was then determined from least-squares fitting of Voigt line shape profiles to the measured data. Transition line strengths were taken from the HITRAN2012 molecular spectroscopic database [41].

2.2 Line selection

The line selection, or rather absorption feature selection, was based on absorbance simulations of the gas composition from Table 1 at atmospheric pressure and various temperatures, using the HITRAN2012 [41] and HITEMP [42] databases. The quantities correspond to the exhaust emission of a typical liquid fuel combustion system, such as a spark ignition engine, and represent a worst-case mixture in the sense that NO concentration is lower than average (0.01%-mol instead of 0.1 mol%), while potentially interfering species concentrations are rather large [43]. The investigated spectral range comprised the fundamental vibration–rotation band of NO ($v = 1 \leftarrow 0$) from 5.0 to 5.8 μm . Figure 1 depicts a small section of that range, from 1924 to 1934 cm^{-1} , for temperatures of 300, 800 and 1300 K. Parasitic absorbance from species other than H₂O, CO₂ and CO is smaller than 8×10^{-4} . The feature we selected for the spectrometer is the lambda-doublet R16.5 (1/2) at 1929.03 cm^{-1} , which is unresolved at atmospheric pressure. It is nearly unblended by CO and CO₂ transitions over the entire temperature range of Fig. 1. Water vapor absorption is monotonic with wavenumber for temperatures below 800 K. In this case, absorption due to H₂O can be incorporated into

the intensity baseline fit (cf. Sect. 2.1), even if the water vapor concentration is unknown. For higher temperatures, the HITEMP line data reveal H₂O lines near the R16.5 transition, which are well within the tuning range of the laser (1.1 cm^{-1} , see Sect. 3.2), and thus could be used for simultaneous H₂O concentration measurement. The air co-flow in this work, however, did not contain significant amounts of water vapor.

The P11.5 (1/2) doublet at 1835.57 cm^{-1} and the R6.5 (1/2) doublet at 1900.08 cm^{-1} , used for NO absorption spectroscopy in [14] and [15, 19, 27, 28] respectively, were also considered to be suitable for measurements in exhaust environments. Like the R16.5 transition, they exhibit negligible parasitic absorption from species other than H₂O, while the water vapor background is also monotonic below 800 K. However, the combined line strength of the R16.5 transition exceeds those of the aforementioned for temperatures above 730 K.

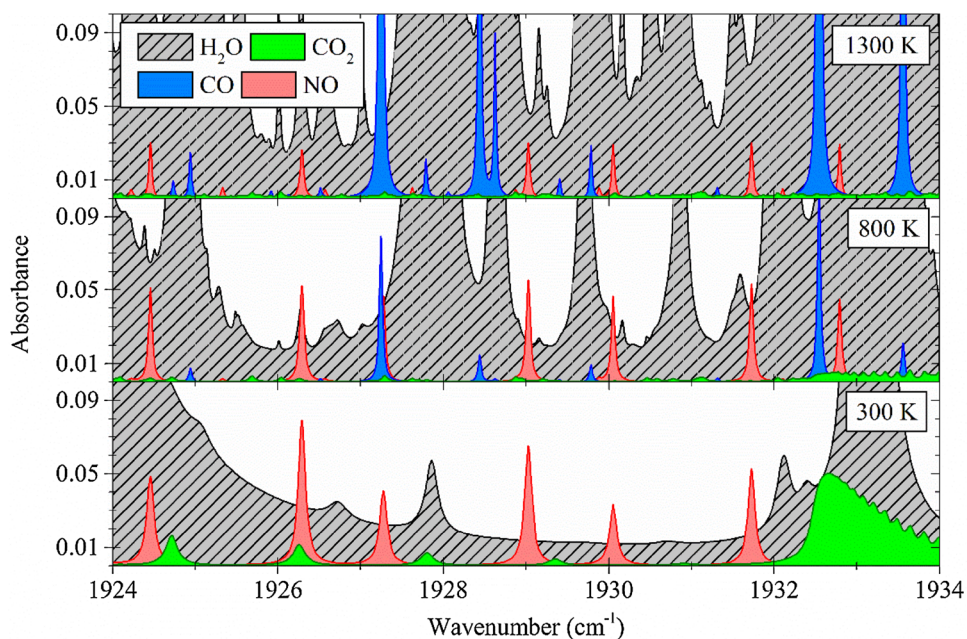
Chao et al. used both R15.5 transitions at 1926.29 cm^{-1} (1/2) and 1927.27 cm^{-1} (3/2) for concentration measurements in the combustion exhaust at the economizer exit of a coal-fired power plant, at a temperature of 620 K [26]. For higher temperatures, these transitions show severe overlapping with H₂O and CO absorption lines, as Chao et al. stated in a previous publication [25].

Table 1 Gas matrix used for spectrum simulations (in molar percentage), with small NO mole fraction and high concentrations of potential mid-infrared absorbers

H ₂ O	CO ₂	CO	NO	NO ₂	N ₂ O	NH ₃	H ₂ CO	CH ₄	C ₂ H ₂	C ₂ H ₄	C ₂ H ₆	SO ₂
15	15	1	0.01	0.1	0.1	0.1	0.01	0.1	0.1	n.a.	n.a.	n.a.

Molecules denoted with n.a. show zero absorption in the spectral range of interest, according to HITRAN2012

Fig. 1 Absorbance simulations of the gas composition from Table 1 at three different temperatures. Only H₂O, CO₂, CO and NO show significant absorbance in the depicted spectral range. The R16.5 transitions form the absorption feature at 1929 cm^{-1} (5184 nm). The data at 800 and 1300 K were taken from the HITEMP database, while at 300 K the HITRAN2012 and HITEMP simulations were practically identical



3 Experimental setup

3.1 Plasma-heated test rig

To prove the feasibility of the NO sensor in a high temperature environment, mole fraction measurements were conducted in a microwave plasma-heated test rig. The test rig was designed for auto-ignition studies of turbulent non-premixed flows, and a detailed report on development and characterization can be found in [39]. Only a brief description will be given here. Essentially, a fuel jet propagates into a hot co-flow of air at atmospheric pressure, and turbulent mixing of fuel and oxidizer leads to auto-ignition. A magnetron with a maximum power of 75 kW is used for plasma heating of the dry air, which is injected into a tube-in-tube system of stainless steel (200 mm inner diameter) and high temperature ceramics (160 mm inner diameter). The air is metered by a system of mass flow controllers, and radial temperature homogenization of the co-flow is achieved by a static mixer. Further downstream at the burner head, which is shown in Fig. 2 (left), the highly turbulent co-flow is contracted and exits a fused silica tube with 82 mm inner diameter. At this point, a fuel jet from a concentrically aligned fuel nozzle (7 mm outer diameter) is injected into the co-flow. At a certain distance from the nozzle, isolated flame kernels emerge. These flame kernels expand while propagating downstream, and eventually form the base of a lifted flame. Regarding only the heated co-flow, operational points of the test rig are characterized by the temperature T_{ctrl} , measured 240 mm upstream from the burner exit, and the bulk velocity u . Temperatures of up to 1300 K and velocities up to 40 m/s can be realized.

As air plasmas at atmospheric pressure produce significant amounts of NO [44], and NO can have an impact on the auto-ignition process such as altering the ignition

temperature [45, 46], its concentration in the co-flow is of particular interest. Eitel et al. measured the NO concentration for various operating points of the test rig by means of an extractive chemiluminescence analyzer (Horiba MEXA 1170NX) [39]. We repeated these measurements using our ICL-based spectrometer, which will be introduced in the following section. Note that in both cases the fuel nozzle was removed from the test rig, to provide a more homogeneous flow profile. Also, because the nozzle protrudes about 5 mm from the burner exit, the beam could be placed closer to the exit in the case of the absorption measurement.

Due to the static mixer inside the flow channel and the high turbulence with Reynolds numbers above 8000, the NO concentration in the co-flow is presumed to be homogeneous for all operating points of the test rig. Temperature on the other hand is not constant in radial direction r . Eitel et al. measured the temperature profile at the burner exit for two operating points: for co-flow control temperatures of 923 and 1273 K at a bulk velocity of 30 m/s [39]. The data for the 1273 K case are plotted in Fig. 2 (right). The profiles show a plateau with temperatures larger than $0.9 \times T_{\text{ctrl}}$ for $r \leq 35$ mm, and a steep decrease in temperature for $35 < r < 41$ mm, due to thermal boundary layers forming inside the fused silica tube. As these measured temperature profiles are very similar, linear interpolation and extrapolation was applied to infer profiles for control temperatures from 773 to 1323 K.

3.2 Spectrometer setup

According to the line selection (Sect. 2.2), a 5184 nm monomode laser was selected to access the R16.5 (1/2) transition at 1929.03 cm^{-1} . The laser is a DFB type ICL manufactured by nanoplus [38] with a maximum output power of ~ 1 mW. Its chip temperature was controlled to

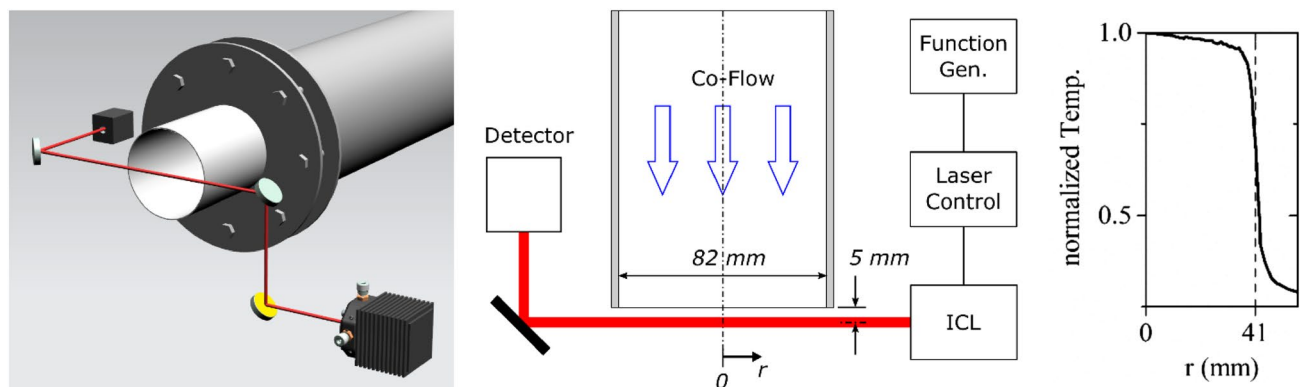


Fig. 2 Left CAD rendering of the spectrometer setup at the co-flow exit of the auto-ignition test rig, with the ICL and collimator in the lower right corner and the detection module in the upper left corner.

Center sectional view (schematic) of the experimental setup. Right normalized temperature profile at the co-flow exit for a control temperature of 1273 K, measured by Eitel et al. [39]

−6.4 °C, and a 2 kHz sawtooth current ramp was applied to scan the wavelength over the entire absorption feature (FWHM $\sim 0.04 \text{ cm}^{-1}$ for the conditions in the test rig). This yielded a tuning range of 1.1 cm^{-1} , sufficiently wide for the intensity baseline fit. The collimated beam (3 mm diameter) traversed the hot air co-flow at an axial distance of 5 mm to the burner head, as it can be seen in Fig. 2 (center). The beam was directed onto a non-cooled, 5 MHz bandwidth HgCdTe photovoltaic detection module (Vigo System). Data acquisition was performed by National Instruments hardware with 16 bit resolution at 2 MSamples/s.

The absorption path length was assumed to equal the 82 mm inner diameter of the burner exit. Ambient pressure was monitored using a Vaisala analog barometer.

The co-flow temperature was measured by a 500 μm bead diameter type N thermocouple positioned 10 mm above the beam, at $r = 0$ in radial direction. At elevated temperatures, accounting for radiative heat loss of the thermocouple wire and bead is indispensable. This is usually done by a simple energy balance on the thermocouple, including only radiation and convection as the most prominent heat transfer mechanisms. However, this procedure is prone to errors, as it is a strongly simplified model with large uncertainties, resulting from uncertainties in the surface emissivity and the correct choice of a Nusselt number correlation [47]. To avoid these uncertainties, we conducted reference measurements in the exit flow of an electric in-line air heater, at various flow velocities and heating powers. The flow temperature was measured accurately using N_2 ro-vibrational CARS (coherent anti-Stokes Raman spectroscopy) [48], and the experiment was then repeated using the aforementioned thermocouple. The accuracy of this correction method (see Sect. 4) is believed to be higher than the accuracy achieved by a conventional ‘radiation

correction’. These reference data were used to correct the measured co-flow temperature, which was then used for scaling the temperature profile for the particular test rig operating point.

For the Voigt line fit, Doppler broadening was calculated using the measured temperature, while pressure broadening coefficients were free parameters due to their high uncertainties of up to 20% in HITRAN2012. A fourth-order polynomial was applied for the intensity baseline fit. The NO concentrations were determined using Eq. (3) by employing the measured temperature profiles from [39]. Evaluation at different path section lengths showed a discretization of $L_i = 0.1 \text{ mm}$ to be sufficiently accurate.

4 Results and discussion

The ICL-based NO sensor was applied for concentration measurements in the plasma-heated co-flow of the test rig for various stationary operating points with co-flow control temperatures ranging from 773 to 1323 K and bulk velocities ranging from 12 to 37 m/s. An exemplary absorbance spectrum for $T_{\text{ctrl}} = 1323 \text{ K}$; $u = 34.3 \text{ m/s}$ is shown in Fig. 3 (left).

At this temperature, the R27.5 (3/2) transitions at 1928.87 cm^{-1} are visible, which were always included in the Voigt fit. Figure 3 (right) shows the measured time series of NO concentrations for this operational point. Fluctuations due to flow inhomogeneities and the closed-loop control of the test rig resulted in a standard deviation of 55 ppm, or 0.6 mol%.

The Allan-Werle deviation σ_A [49] for this operating point (Fig. 4) showed the white noise regime to end after a measurement time of only 10 ms. This is due to small periodic concentration fluctuations (cycle duration

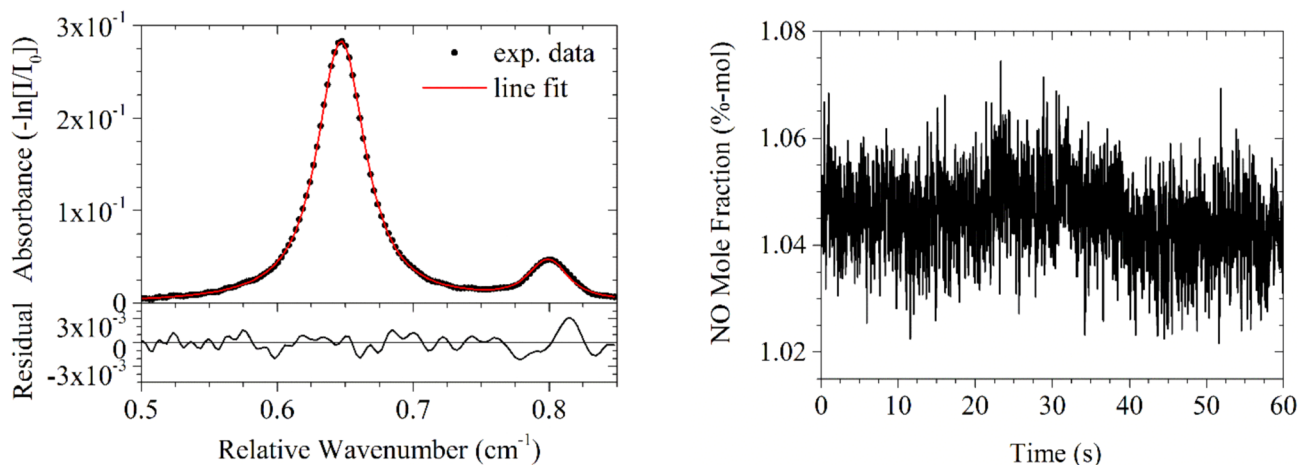


Fig. 3 Left measured absorbance (20 averages) at 1323 K and 34.3 m/s, yielding an NO mole fraction of 1.05 mol%. Right corresponding time series for this operating point

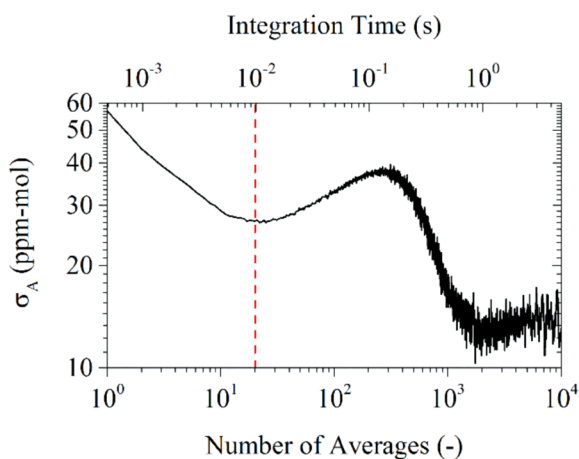


Fig. 4 Allan-Werle deviation for the operating point (1323 K; 34.3 m/s). A pre-averaging of 20 laser scans was chosen, to optimize the signal-to-noise ratio

≈ 0.25 s), supposedly caused by a fluctuating plasma volume. The minimum Allan-Werle deviation is observed at an integration time of 1 s, when these changes in concentration are averaged out. We chose to stay within the white noise regime, thus only 20 consecutive scans were averaged before evaluation, yielding a temporal resolution of 100 Hz.

The data were post-processed using a moving average filter, to remove high frequency fringes due to an etalon effect between the beam collimator and the detector. Tilting the detector with respect to the beam did not mitigate the effect. The highly reflecting hyperhemispherical GaAs lens which the detector material is immersed in is believed to be the reason for this behavior. However, the detector can be placed at a large distance to the collimator, resulting

in a small amplitude (low etalon finesse), high frequency (small free spectral range) interference pattern, which does not distort the absorption spectrum significantly. The noise-equivalent sensitivity (1σ) is in this case 70 ppm, or ~ 6 ppm m and ~ 600 ppb $m/\sqrt{\text{Hz}}$.

NO mole fractions have been measured for several operational points, and were averaged over a time period of 60 s to compare against the gas analyzer results from [39]. Measured mole fractions as a function of co-flow velocity for different control temperatures are depicted in Fig. 5, left for the absorption sensor and right for the extractive gas analyzer. Standard deviations are below 1.5% in any case. The trends obviously are similar: lower NO mole fraction at higher flow velocity and higher mole fraction at higher temperature. Low flow velocity reduces the residence time of the fluid inside the plasma, thus less NO is produced. On the other hand, high flow temperature is caused by high microwave heating power, promoting a larger plasma volume and more NO production [39]. Due to the temperature dependence of line strength, the best sensitivity is reached at the 773 K set points, where we observed a noise equivalent detection limit (1σ) of 30 ppm, or ~ 2.5 ppm m and ~ 250 ppb $m/\sqrt{\text{Hz}}$.

As the temperature set points do not completely coincide in both measurements, the temperature dependence of the concentration was evaluated for fixed co-flow velocities (marked by vertical dashed lines in Fig. 5), using a cubic spline interpolation between the velocity set points for each temperature. Figure 6 shows these plots for the velocities 20, 24 and 28 m/s. Both measurement techniques show a linear behavior and good agreement in the lower temperature range. For temperatures above 1000 K, the spectroscopically measured concentrations exceed those from the gas analyzer by up to 16 mol%, while the latter depart from linearity. Note that

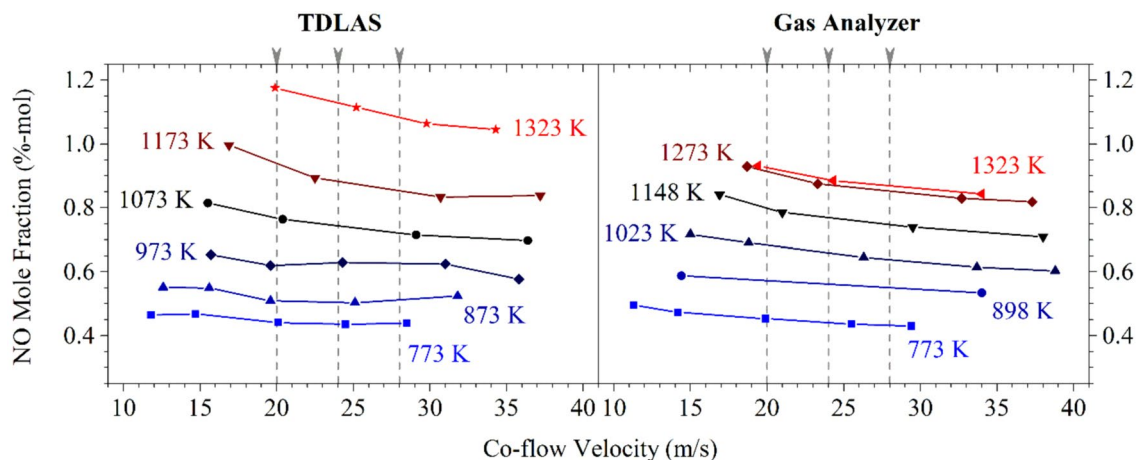


Fig. 5 NO mole fraction in the co-flow as a function of bulk velocity and temperature. *Left* measured by the ICL-based sensor. *Right* measured by a commercial gas analyzer. For comparison, an interpolation was applied along the *vertical dashed lines*. Those results are shown in Fig. 6

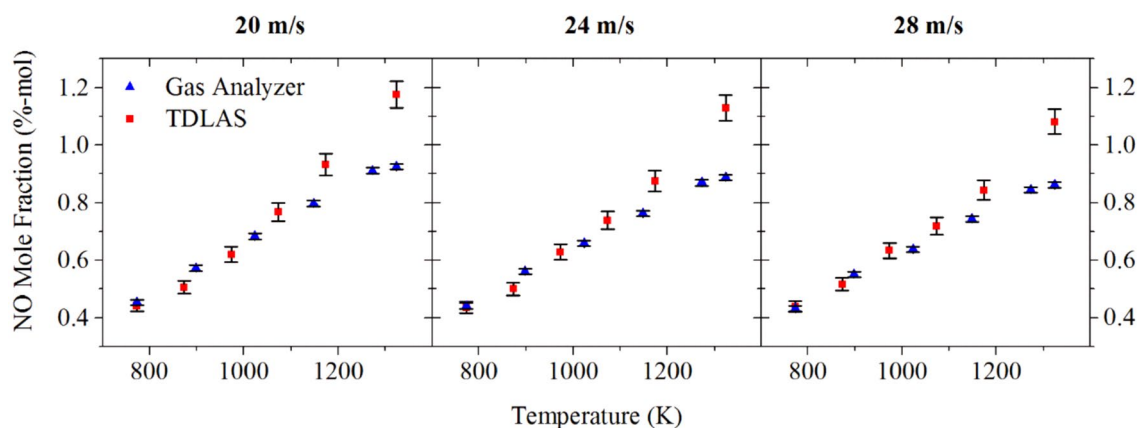


Fig. 6 NO mole fractions over temperature, interpolated from the data in Fig. 4, for co-flow bulk velocities of 20, 24 and 28 m/s (from left to right) for both measurement techniques

the error bars do not indicate the standard deviation, but the accuracy of the measurement device. The manufacturer of the analyzer specifies a linearity error within $\pm 1\%$ of full scale, which equals a mole fraction of ± 100 ppm in this case. The total error of the spectroscopic measurements was estimated as follows. Error in absorption length was assumed to be 1 mm (or 1.2%), as the co-flow starts to spread after exiting the fused silica tube. Temperature error is expected to be 10 K due to uncertainty in the thermocouple reference measurements, plus 2%, which is the accuracy of the CARS measurement system. The error in line shape area was neglected due to the high signal-to-noise ratios (compare Fig. 3, left). By far the largest error stems from 10% uncertainty in line strength, according to HITRAN2012. This uncertainty, however, would produce a systematic deviation from the gas analyzer measurements, which cannot be observed for lower temperatures. Line strength error is thus not included in Fig. 6. Run-to-run stability of the test rig can also not be responsible for the difference between the two techniques, as it was characterized by repeated gas analyzer measurements, yielding only $\pm 2\%$ in NO mole fraction [39]. We suspect sampling effects of the intrusive gas analyzer to be the major source of the discrepancy. Besides, at the higher temperatures, the mole fractions measured by the gas analyzer come close to the maximum of its measuring range, which is 1.0 mol%. Examining these potential systematic errors of sampling techniques, however, is beyond the scope of this study.

5 Conclusion

An in situ NO sensor based on a mid-infrared DFB interband cascade laser was presented. The ruggedness and simplicity of the components enable applications in industrial combustion exhaust systems. First measurements were conducted in

a well-characterized laboratory auto-ignition test rig. At temperatures below 1000 K, the measured mole fractions show excellent agreement with results from a commercial sampling gas analyzer. The cause for the observed discrepancies at higher temperatures (up to 1323 K) is not ultimately clear, but we are confident about the stated accuracy of the spectroscopic measurements, due to the careful consideration of radiation correction of the thermocouple as well as incorporating the inhomogeneous temperature profile along the optical path. The demonstrated detection limit was as low as 250 ppb m/\sqrt{Hz} , which can be further improved by eliminating back reflections from the detection system. The primary advantage over recently presented mid IR diode laser sensors is the use of the R16.5 transition, making this sensor suitable for low interference measurements in exhaust gases over a wide range of temperatures and species compositions.

Acknowledgements We gratefully acknowledge the support by the Fritz und Margot Faudi-Stiftung through Project No. 91. A. Dreizler is grateful for general support by the Gottfried Wilhelm Leibniz Program of the Deutsche Forschungsgemeinschaft.

References

1. J. Warnatz, U. Maas, R.W. Dibble, *Combustion* (Springer, Berlin, 2006)
2. J.H. Seinfeld, S.N. Pandis, *Atmospheric chemistry and physics* (Wiley, Hoboken, 2016)
3. P.J. Barnes, R.A. Dweik, A.F. Gelb, P.G. Gibson, S.C. George, H. Grasemann, I.D. Pavord, F. Ratjen, P.E. Silkoff, D.R. Taylor, N. Zamel, *Chest* (2010). doi:10.1378/chest.09-2090
4. M.G. Allen, *Meas. Sci. Technol.* **9**, 545 (1998)
5. J. Hodgkinson, R.P. Tatam, *Meas. Sci. Technol.* (2013). doi:10.1088/0957-0233/24/1/012004
6. S.F. Hanna, R. Barron-Jimenez, T.N. Anderson, R.P. Lucht, J.A. Caton, T. Walther, *Appl. Phys. B* (2002). doi:10.1007/s00340-002-0974-9

7. D.B. Oh, A.C. Stanton, *Appl. Opt.* (1997). doi:[10.1364/AO.36.003294](https://doi.org/10.1364/AO.36.003294)
8. D.M. Sonnenfroh, M.G. Allen, *Appl. Opt.* (1997). doi:[10.1364/AO.36.007970](https://doi.org/10.1364/AO.36.007970)
9. P.K. Falcone, R.K. Hanson, C.H. Kruger, *Combust. Sci. Technol.* (1983). doi:[10.1080/00102208308923704](https://doi.org/10.1080/00102208308923704)
10. T.N. Anderson, R.P. Lucht, R. Barron-Jimenez, S.F. Hanna, J.A. Caton, T. Walther, S. Roy, M.S. Brown, J.R. Gord, I. Critchley, L. Flamand, *Appl. Opt.* (2005). doi:[10.1364/AO.44.001491](https://doi.org/10.1364/AO.44.001491)
11. T.N. Anderson, R.P. Lucht, S. Priyadarsan, K. Annamalai, J.A. Caton, *Appl. Opt.* (2007). doi:[10.1364/AO.46.003946](https://doi.org/10.1364/AO.46.003946)
12. F. Capasso, *Opt. Eng.* (2010). doi:[10.1117/1.3505844](https://doi.org/10.1117/1.3505844)
13. J. Jágorská, P. Jouy, B. Tuzson, H. Looser, M. Mangold, P. Soltic, A. Hugi, R. Brönnimann, J. Faist, L. Emmenegger, *Opt. Express* (2015). doi:[10.1364/OE.23.001512](https://doi.org/10.1364/OE.23.001512)
14. Y.A. Bakirkin, A.A. Kosterev, R.F. Curl, F.K. Tittel, D.A. Yarekha, L. Hvozdar, M. Giovannini, J. Faist, *Appl. Phys. B* (2006). doi:[10.1007/s00340-005-2058-0](https://doi.org/10.1007/s00340-005-2058-0)
15. L. Dong, V. Spagnolo, R. Lewicki, F.K. Tittel, *Opt. Express* (2011). doi:[10.1364/OE.19.024037](https://doi.org/10.1364/OE.19.024037)
16. V.L. Kasuytich, R.J. Holdsworth, P.A. Martin, *Appl. Phys. B* (2008). doi:[10.1007/s00340-008-3097-0](https://doi.org/10.1007/s00340-008-3097-0)
17. A.A. Kosterev, A.L. Malinovsky, F.K. Tittel, C. Gmachl, F. Capasso, D.L. Sivco, J.N. Baillargeon, A.L. Hutchinson, A.Y. Cho, *Appl. Opt.* (2001). doi:[10.1364/AO.40.005522](https://doi.org/10.1364/AO.40.005522)
18. M.R. McCurdy, Y.A. Bakirkin, F.K. Tittel, *Appl. Phys. B* (2006). doi:[10.1007/s00340-006-2365-0](https://doi.org/10.1007/s00340-006-2365-0)
19. J.B. McManus, D.D. Nelson, S.C. Herndon, J.H. Shorter, M.S. Zahniser, S. Blaser, L. Hvozdar, A. Muller, M. Giovannini, J. Faist, *Appl. Phys. B* (2006). doi:[10.1007/s00340-006-2407-7](https://doi.org/10.1007/s00340-006-2407-7)
20. D.D. Nelson, J.H. Shorter, J.B. McManus, M.S. Zahniser, *Appl. Phys. B Lasers Opt.* (2002). doi:[10.1007/s00340-002-0979-4](https://doi.org/10.1007/s00340-002-0979-4)
21. C. Roller, K. Namjou, J. Jeffers, W. Potter, P.J. McCann, J. Grego, *Opt. Lett.* (2002). doi:[10.1364/OL.27.000107](https://doi.org/10.1364/OL.27.000107)
22. M.L. Silva, D.M. Sonnenfroh, D.I. Rosen, M.G. Allen, A.O. Keefe, *Appl. Phys. B* (2005). doi:[10.1007/s00340-005-1922-2](https://doi.org/10.1007/s00340-005-1922-2)
23. V. Spagnolo, A.A. Kosterev, L. Dong, R. Lewicki, F.K. Tittel, *Appl. Phys. B* (2010). doi:[10.1007/s00340-010-3984-z](https://doi.org/10.1007/s00340-010-3984-z)
24. W.H. Weber, J.T. Remillard, R.E. Chase, J.F. Richter, F. Capasso, C. Gmachl, A.L. Hutchinson, D.L. Sivco, J.N. Baillargeon, A.Y. Cho, *Appl. Spectrosc.* (2002). doi:[10.1366/000370202760077414](https://doi.org/10.1366/000370202760077414)
25. X. Chao, J.B. Jeffries, R.K. Hanson, *Proc. Combust. Inst.* (2011). doi:[10.1016/j.proci.2010.05.014](https://doi.org/10.1016/j.proci.2010.05.014)
26. X. Chao, J.B. Jeffries, R.K. Hanson, *Appl. Phys. B* (2012). doi:[10.1007/s00340-011-4839-y](https://doi.org/10.1007/s00340-011-4839-y)
27. S. Wehe, M. Allen, Xiang Liu, J. Jeffries, R. Hanson, *Proc. IEEE Sens. (IEEE Cat. No.03CH37498)* (2003). doi:[10.1109/ICSENS.2003.1279052](https://doi.org/10.1109/ICSENS.2003.1279052)
28. G. Wysocki, A.A. Kosterev, F.K. Tittel, *Appl. Phys. B* (2005). doi:[10.1007/s00340-005-1764-y](https://doi.org/10.1007/s00340-005-1764-y)
29. R. Lewicki, J.H. Doty, R.F. Curl, F.K. Tittel, G. Wysocki, *Proc. Natl. Acad. Sci. USA* (2009). doi:[10.1073/pnas.0906291106](https://doi.org/10.1073/pnas.0906291106)
30. Z. Li, C. Shi, W. Ren, *Opt. Lett.* (2016). doi:[10.1364/OL.41.004095](https://doi.org/10.1364/OL.41.004095)
31. R.Q. Yang, *Superlattices Microstruct.* (1995). doi:[10.1006/spmi.1995.1017](https://doi.org/10.1006/spmi.1995.1017)
32. I. Vurgaftman, R. Weih, M. Kamp, J.R. Meyer, C.L. Canedy, C.S. Kim, M. Kim, W.W. Bewley, C.D. Merritt, J. Abell, S. Höfling, *J. Phys. D Appl. Phys.* (2015). doi:[10.1088/0022-3727/48/12/123001](https://doi.org/10.1088/0022-3727/48/12/123001)
33. L. Dong, F.K. Tittel, C. Li, N.P. Sanchez, H. Wu, C. Zheng, Y. Yu, A. Sampaolo, R.J. Griffin, *Opt. Express* (2016). doi:[10.1364/OE.24.00A528](https://doi.org/10.1364/OE.24.00A528)
34. L. Dong, Y. Yu, C. Li, S. So, F.K. Tittel, *Opt. Express* (2015). doi:[10.1364/OE.23.019821](https://doi.org/10.1364/OE.23.019821)
35. S. Lundqvist, P. Kluczynski, R. Weih, M. von Edlinger, L. Nahle, M. Fischer, A. Bauer, S. Hofling, J. Koeth, *Appl. Opt.* (2012). doi:[10.1364/AO.51.006009](https://doi.org/10.1364/AO.51.006009)
36. K.M. Manfred, G.A.D. Ritchie, N. Lang, J. Röpcke, J.H. van Helden, *Appl. Phys. Lett.* (2015). doi:[10.1063/1.4922149](https://doi.org/10.1063/1.4922149)
37. R. Sur, S. Wang, K. Sun, D.F. Davidson, J.B. Jeffries, R.K. Hanson, *J. Quant. Spectrosc. Radiat. Transf.* (2015). doi:[10.1016/j.jqsrt.2015.01.023](https://doi.org/10.1016/j.jqsrt.2015.01.023)
38. M. von Edlinger, J. Scheuermann, R. Weih, C. Zimmermann, L. Nahle, M. Fischer, J. Koeth, S. Hofling, M. Kamp, *IEEE Photon. Technol. Lett.* (2014). doi:[10.1109/LPT.2013.2297447](https://doi.org/10.1109/LPT.2013.2297447)
39. F. Eitel, J. Pareja, D. Geyer, A. Johchi, F. Michel, W. Elsaßer, A. Dreizler, *Exp. Fluids* (2015). doi:[10.1007/s00348-015-2059-7](https://doi.org/10.1007/s00348-015-2059-7)
40. H. Teichert, T. Fernholz, V. Ebert, *Appl. Opt.* (2003). doi:[10.1364/AO.42.002043](https://doi.org/10.1364/AO.42.002043)
41. L.S. Rothman, I.E. Gordon, Y. Babikov, A. Barbe, D. Chris Benner, P.F. Bernath, M. Birk, L. Bizzocchi, V. Boudon, L.R. Brown, A. Campargue, K. Chance, E.A. Cohen, L.H. Coudert, V.M. Devi, B.J. Drouin, A. Fayt, J.-M. Flaud, R.R. Gamache, J.J. Harrison, J.-M. Hartmann, C. Hill, J.T. Hodges, D. Jacquemart, A. Jolly, J. Lamouroux, R.J. Le Roy, G. Li, D.A. Long, O.M. Lyulin, C.J. Mackie, S.T. Massie, S. Mikhailenko, H. Müller, O.V. Naumenko, A.V. Nikitin, J. Orphal, V. Perevalov, A. Perrin, E.R. Polovtseva, C. Richard, M. Smith, E. Starikova, K. Sung, S. Tashkun, J. Tennyson, G.C. Toon, V. Tyuterev, G. Wagner, *J. Quant. Spectrosc. Radiat. Transf.* (2013). doi:[10.1016/j.jqsrt.2013.07.002](https://doi.org/10.1016/j.jqsrt.2013.07.002)
42. L.S. Rothman, I.E. Gordon, R.J. Barber, H. Dothe, R.R. Gamache, A. Goldman, V.I. Perevalov, S.A. Tashkun, J. Tennyson, *J. Quant. Spectrosc. Radiat. Transf.* (2010). doi:[10.1016/j.jqsrt.2010.05.001](https://doi.org/10.1016/j.jqsrt.2010.05.001)
43. G.P. Merker, C. Schwarz, R. Teichmann, *Grundlagen Verbrennungsmotoren* (Vieweg + Teubner, Wiesbaden, 2012)
44. M. Leins, L. Alberts, M. Kaiser, M. Walker, A. Schulz, U. Schumacher, U. Stroth, *Plasma Process. Polym.* (2009). doi:[10.1002/ppap.200930604](https://doi.org/10.1002/ppap.200930604)
45. K. Takita, N. Abe, G. Masuya, Y. Ju, *Proc. Combust. Inst.* (2007). doi:[10.1016/j.proci.2006.07.108](https://doi.org/10.1016/j.proci.2006.07.108)
46. Y. Tan, C.G. Fotache, C.K. Law, *Combust. Flame* (1999). doi:[10.1016/S0010-2180\(99\)00064-4](https://doi.org/10.1016/S0010-2180(99)00064-4)
47. C.R. Shaddix, in *Proceedings of the 33rd National Heat Transfer Conference*
48. A. Singh, M. Mann, T. Kissel, J. Brübach, A. Dreizler, *Flow Turbul. Combust.* (2013). doi:[10.1007/s10494-011-9384-6](https://doi.org/10.1007/s10494-011-9384-6)
49. P. Werle, R. Mücke, F. Slemr, *Appl. Phys. B* (1993). doi:[10.1007/BF00425997](https://doi.org/10.1007/BF00425997)